Fault Current Tracing and Identification via Machine Learning Considering Distributed Energy Resources in Distribution Networks †

Wanghao Fei and Paul Moses *

School of Electrical and Computer Engineering, University of Oklahoma, Norman, OK 73019, USA; whf@ou.edu
* Correspondence: pmoses@ou.edu
† This paper is an extended version of our paper published in In Proceedings of the 2019 IEEE 7th International Conference on Smart Energy Grid Engineering (SEGE), Oshawa, ON, Canada, 12–14 August 2018; pp. 196–200.

Abstract: The growth of intermittent distributed energy sources (DERs) in distribution grids is raising many new operational challenges for utilities. One major problem is the back feed power flows from DERs that complicate state estimation for practical problems, such as detection of lower level fault currents, that cause the poor accuracy of fault current identification for power system protection. Existing artificial intelligence (AI)-based methods, such as support vector machine (SVM), are unable to detect lower level faults especially from inverter-based DERs that offer limited fault currents. To solve this problem, a current tracing method (CTM) has been proposed to model the single distribution feeder as several independent parallel connected virtual lines that traces the detailed contribution of different current sources to the power line current. Moreover, for the first time, the enhanced current information is used as the expanded feature space of SVM to significantly improve fault current detection on the power line. The proposed method is shown to be sensitive to very low level fault currents which is validated through simulations.

Keywords: current tracing; fault current; distributed energy resources; network model

1. Introduction

Due to the increasing penetration rate of distributed energy sources (DERs), such as solar power injected at the distribution side of the power system, during the past decade, distribution grids have become large, complex, interconnected networks. The infusion of DERs onto distribution grids raises some new state estimation challenges, such as fault current identification, which was less of an issue in conventional distribution grids operating without DERs.

The traditional distribution grid was not affected by irregular back power feeds caused by intermittent DER activity, as it was originally designed for single direction power flow from the substation to the customers. The ordinary fault current identification process is based on the fault current threshold where no DERs are injected into the distribution grid. With DERs, excess power can be generated and consumed by the customer or feed back to the distribution feeder. This raises new challenges, especially in grid modeling methods for fault current identification, where the impact of back feed power flow has to be considered for determining the fault current threshold. Failure to do so may have far reaching and costly consequences such as inadvertent tripping of circuits or overlooking faults in the system.

Researchers have proposed many grid modeling methods for different types of power grids such as averaged models [1,2] and the port-Hamiltonian-based dynamic power system model [3].

Certain modeling methods are suited for specific parts of the grid such as cyber-physical power systems framework modeling [4,5], topology modeling [6,7], load flow modeling [8,9], lightning protection models [10], and traveling wave modeling [11]. In [12,13], the author used pattern recognition to identify the fault current with the waveform data, which is an efficient tool for power transmission line fault detection. In addition, with the benefit of fast developing artificial intelligence (AI) technologies, many AI-based power system fault identification methods have been proposed as well, such as support vector machine (SVM) [14], k-nearest neighbors algorithm (KNN) [13], pattern recognition [15], and deep learning [16].

Although different AI methods have been used to improve the accuracy of power system fault identification, the approaches still heavily rely on grid modeling methods for some part of the power grid. Most importantly, almost all of these AI-based fault current identification methods based on existing grid modeling methods totally depend on the existing power line infrastructure, in that currents from different power sources are congested to one end of a single power line and flow towards the other end [17–19]. These methods are very effective when it comes to the identification of larger fault currents, but some detailed current information such as those from inverter-based DERs are difficult to detect. A much more detailed grid modeling method is needed to augment the AI method to be more sensitive to detect some lower level faults. This is particularly important in modern distribution grids, as inverter-based DERs are known to produce exceptionally small fault current contributions, due to inverter current limiting action, and are very difficult to detect through conventional means.

For addressing the aforementioned grid modeling problems, a detailed grid model (referred to herein as the CTM) was proposed by the authors in a companion paper [20], which has sufficient detail of the current flows on the power line from each individual DER connected to the grid. The main objectives of this paper are as follows. First, for the first time, it is shown how the accuracy of implementing AI algorithms on such a detailed grid model can be improved. Specifically, implementing SVM algorithm on the proposed CTM model is explored. Second, in addition to using fault current flows as the only input feature, the "traced" current information to expand the dimension of the feature space is exploited. That is, the traced current is used along with the power line current as the expanded feature space to identify the fault current which is a departure from existing methods. Finally, the performance of the combination of CTM with the SVM is demonstrated in the practical scenario of fault identification with DERs operating in distribution grids. Specifically, this work shows how applying this hybrid method can improve sensitivity in detecting very low level faults.

This paper is organized as follows. In Section 2, the weaknesses of using traditional grid models for fault current identification are pointed out, and applying CTM for multiple current sources of a distribution grid is proposed. The SVM method is implemented for fault current identification using the traced current in Section 3. Simulation results are presented in Section 4 and are discussed in Section 5, with concluding remarks given in Section 6.

2. Proposed Tracing Method

2.1. Single Power Line Fault Current Threshold

Consider the case where a DER group consists for example of solar and wind generation, a vehicle-to-grid support battery storage, and loads that are attached to bus 1 are connected to the end of the power distribution grid through a single power line as shown in Figure 1.
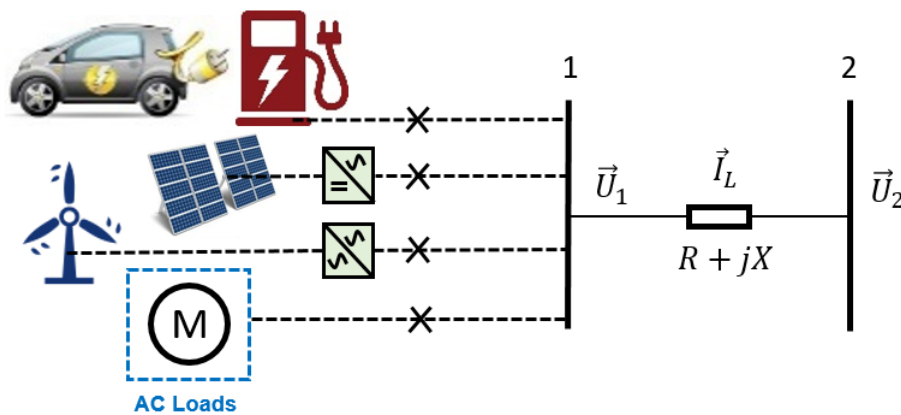
Figure 1. Single power line with distributed energy source (DER) customers.

In Figure 1, $\vec{I}_L$ represents the power line current, and $\vec{U}_1$ and $\vec{U}_2$ are the voltages on buses 1 and 2, respectively. The applied voltage difference angle of $\vec{U}_1 - \vec{U}_2$ is ψ. Without the impact of the DER group, $\vec{I}_L$ flows from bus 2 to bus 1 and the fault current can be easily identified by setting the fault current threshold. However, when the impact of renewable energy sources is considered, as in this case, the fault current threshold is difficult to determine, as the DERs may contribute to the fault current and the detection threshold varies. The power line's current value and direction may also vary with the impact of DERs, which complicates the discrimination of faults from the normal condition. It is therefore necessary to know significantly more details of the current to determine if there is a fault on the power line or at the load.

2.2. Current Tracing

Using Figure 1 to demonstrate the CTM deduction, without loss of generality, it is assumed that the power line impedance is

$$Z = R + jX, \tag{1}$$

where $R > 0$ and $X > 0$ are the resistance and reactance of the power line, respectively. An alternative case, when $X < 0$, is discussed in the companion conference paper [20]. In this paper, only the $X > 0$ case is considered. The impedance angle is θ. Based on Kirchhoff's current law, it follows that

$$\vec{I}_L = \sum I_i e^{j\phi_i}. \tag{2}$$

where $\vec{I}_i = I_i e^{j\phi_i}$ is the current of the ith DER, and $I_i > 0$ and ϕ_i are the magnitude and phase angle of $\vec{I}_i$, respectively.

Figure 1 can be expressed with an equivalent circuit as shown in Figure 2a. The equivalence holds as shown in Equations (3) and (4):

$$R_E = \frac{R^2 + X^2}{R}, \tag{3}$$

$$X_E = \frac{R^2 + X^2}{X}, \tag{4}$$

where $R_E > 0$ and $X_E > 0$ are the equivalent resistance and reactance respectively. Naturally, the equivalent circuit has the same total resistance, current, and power of the original circuit.
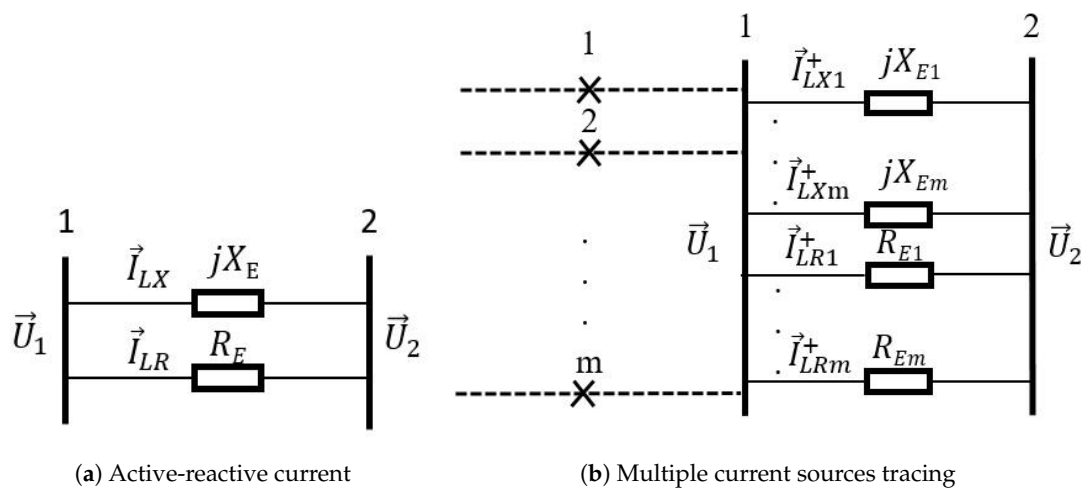
(**a**) Active-reactive current   (**b**) Multiple current sources tracing

Figure 2. Equivalent circuit.

In the equivalent circuit, the power line current $\vec{I}_L$ is virtually split into two parts defined as active current $\vec{I}_{LR}$ and reactive current $\vec{I}_{LX}$, which flows through R_E and X_E, respectively:

$$\vec{I}_L = \vec{I}_{LR} + \vec{I}_{LX}, \tag{5}$$

$$\vec{I}_{LR} = I_{LR}e^{j\psi}, \tag{6}$$

$$I_{LR} = I_L cos(\theta), \tag{7}$$

$$\vec{I}_{LX} = I_{LX}e^{j(\psi - \frac{\pi}{2})}, \tag{8}$$

$$I_{LX} = I_L sin(\theta), \tag{9}$$

where I_{LR} and I_{LX} are the magnitude of the active current and reactive current, respectively. Likewise, all current sources attached to bus 1 follow the same rule:

$$\vec{I}_i = \vec{I}_{Ri} + \vec{I}_{Xi} = I_{Ri}e^{j\psi} + I_{Xi}e^{j(\psi - \frac{\pi}{2})}, \tag{10}$$

$$I_{Ri} = I_{Li}cos(\psi - \phi_i), \tag{11}$$

$$I_{Xi} = I_{Li}sin(\psi - \phi_i), \tag{12}$$

where I_{Ri} and I_{Xi} are the magnitude of the active and reactive current from $\vec{I}_i$, respectively, which could either be positive or negative. From Kirchhoff's current law,

$$\sum_{I_{Ri}>0} (\vec{I}_{Ri}) + \sum_{I_{Ri}<0} (\vec{I}_{Ri}) = \sum (\vec{I}_{Ri}) = \vec{I}_{LR}, \tag{13}$$

$$\sum_{I_{Xi}>0} (\vec{I}_{Xi}) + \sum_{I_{Xi}<0} (\vec{I}_{Xi}) = \sum (\vec{I}_{Xi}) = \vec{I}_{LX}, \tag{14}$$

where $\sum_{I_{Ri}>0} (\vec{I}_{Ri})$ and $\sum_{I_{Ri}<0} (\vec{I}_{Ri})$ stand for the positive and negative part of $\vec{I}_{LR}$, respectively, and $\sum_{I_{Xi}>0} (\vec{I}_{Xi})$ and $\sum_{I_{Xi}<0} (\vec{I}_{Xi})$ represent the positive and negative part of $\vec{I}_{LX}$, respectively. The positive part is responsible for supplying the load as well as feeding extra current to the power distribution grid.

The negative part is responsible for absorbing current from positive part. The jth positive current source flowing through the power line is

$$\vec{I}_{LRj}^+ = I_{LRj}^+ e^{j\psi},\tag{15}$$

$$\vec{I}_{LXj}^+ = I_{LXj}^+ e^{j\left(\psi - \frac{\pi}{2}\right)},\tag{16}$$

$$I_{LRj}^+ = \frac{I_{LR}I_{Rj}}{\sum\limits_{I_{Ri}>0}(I_{Ri})},\tag{17}$$

$$I_{LXj}^+ = \frac{I_{LX}I_{Xj}}{\sum\limits_{I_{Xi}>0}(I_{Xi})}.\tag{18}$$

where $\vec{I}_{LRj}^+$ is the active part of the jth positive current source flowing through the power line with magnitude of I_{LRj}^+, and $\vec{I}_{LXj}^+$ is the reactive part of the jth positive current source flowing through the power line with magnitude of I_{LXj}^+. Therefore, the distribution grid model where each of the currents are independent from one another can be shown in Figure 2b.

Combining the active and reactive components of the jth positive current source flowing through the power line, the equivalent circuit with part of the jth positive current source that flows through the power line can also be derived such that $\vec{I}_{LZj}^+ = \vec{I}_{LRj}^+ + \vec{I}_{LXj}^+$, with its impedance, Z_{Ej}, as shown in Figure 3. The complete derivation of this situation can be found in the companion paper [20].
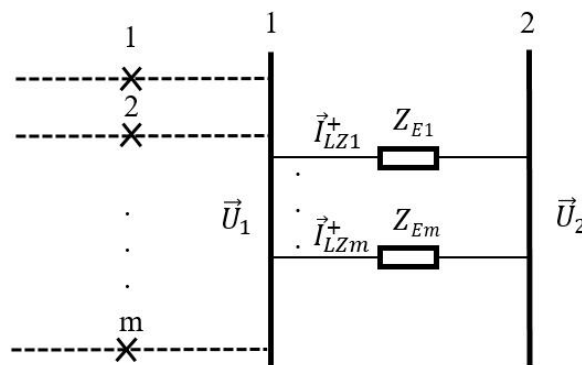

Figure 3. Equivalent circuit of impedance lines.

3. Support Vector Machine and Current Tracing Kernel

3.1. Binary Classification Problem Formation

Given a set of power line current measurements $Z = \{z_i, i = 1...n\}$, $z_i \in \mathbb{R}^m$ that may or may not contain fault current and the set of labels $Y = \{y_i, i = 1...n\}$, $y_i \in \{0,1\}$, m stands for the dimension of the measurement, and n is the number of observations. The fault current identification problem can be modeled as a binary classification problem by establishing the connection between the above two sets such that

$$y_i = \begin{cases} -1 & \text{if } a_i = 0, \\ 1 & \text{if } a_i \neq 0. \end{cases}\tag{19}$$

$y_i = 1$ indicates that the ith current measurement is fault current, or, alternatively, there are no fault currents for $y_i = -1$.

3.2. Support Vector Classifiers

The classification problem is reformatted into the optimization problem in [21]. The objective function can be defined as

$$\texttt{min} \quad \frac{1}{2}||\omega||^2 + C\sum_{i=1}^{m} \xi_i, \tag{20}$$

where C is used to control the penalty of the misclassification, ω is a constant such that $\omega = [\omega_0, \omega_1, ... \omega_m]^T$, and ξ_i is the slack variable. The objective function is subject to the constraint that

$$\omega_0 + \omega^T z_i \geq 1 - \xi_i \; if \; y_i = 1, \tag{21}$$
$$\omega_0 + \omega^T z_i \leq \xi_i - 1 \; if \; y_i = -1. \tag{22}$$

3.3. Support Vector Machines

As an extension of the support vector classifier, SVM is established by enlarging the feature space using kernel. Kernel is a function that is used to quantify the similarity of two observations. A linear Kernel is defined as the inner product of two observations [21]:

$$K(z_i, z_{i'}) = \sum_{j=1}^{m} z_{i,j} z_{i',j}, \tag{23}$$

where z_i and $z_{i'}$ are the two observations, and $z_{i,j}$ and $z_{i',j}$ are the observations on jth dimension.

In addition, some commonly used kernels are [21]

- Polynomial kernel: $K(z_i, z_{i'}) = (1 + \sum_{j=1}^{m} z_{i,j} z_{i',j})^d$
- Radial kernel: $K(z_i, z_{i'}) = exp(-\gamma \sum_{m}^{j=1} (x_{i,j} - x_{i',j})^2)$

where γ and d are positive constants and r is a constant.

3.4. Current Tracing Kernel

In [22], the author applied principle component analysis to select the best features with highest information content to identify faults. This study concluded that the top three features for fault identification were reactive power, real power, and angle of voltage. Interestingly, current is not one of them. The author concluded that with all of the three selected features, the accuracy of identification is almost 96%. With all of the six features, i.e., the above features plus magnitude and angle of current and magnitude of voltage, the accuracy of identification is no more than 97%. In the proposed approach, current is used as the only feature. Without current tracing, the feature space consists of only the line current magnitude and angle.

Based on Equations (15)–(18), the line current can be decomposed into several traced currents flowing through virtual impedance lines as shown in Figure 3. The feature space of line currents can be enlarged by using the traced currents:

$$K(I_L, e^{j(\psi - \theta)}) = \vec{I}_{LZj}^{+}. \tag{24}$$

where K represents the linear mapping from power line current to the traced current.

4. Simulation Results

4.1. Current Tracing Kernel Results

In this simulation, the proposed CTM is applied to the single line system of Figure 4. Both sides of the single line have a group of DERs and loads, and bus 2 is connected directly to the external distribution grid. All of the loads are of the constant power type, and the DERs are static generators.
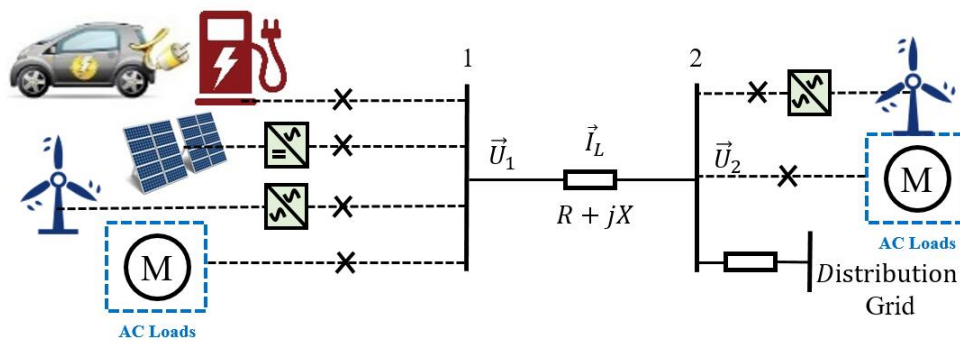
Figure 4. Multiple source to multiple source on single power line.

The current sources parameters are listed in Table 1, which are given in the format of active and reactive power. DERs that connect to bus 1 cannot support the AC loads attached to bus 1 so that the currents flow from bus 2 to bus 1, which is opposite from the case shown in the companion paper [20]. Bus 2 is selected as the reference bus and the single power line is 20 km length with series impedance of 0.121 + j0.107 Ω/km.

Table 1. The current source parameters.

Bus	Label	Power	
		Active/MW	**Reactive/MVar**
1	1	−20	−10
	2	−20	−5
	3	30	15
	4	20	5
2	1	−20	−10
	2	40	15
	3	30.872544	10.771589

In Table 1, the positive elements indicate an absorption of power whereas negative elements represents generating power. The third current source attached to bus 2 is the external grid and is calculated by the power flow. Equations (15) and (16) are applied to find the traced current on the power line from each bus as shown in Table 2. All of the traced currents are listed in per unit value. The traced current magnitude and phase in radians are selected as the kernel for fault current identification.

Table 2. Current tracing results with Equations (15)–(18).

Bus	Label	Active Current Tracing		Reactive Current Tracing	
		Mag	**Phase/°**	**Mag**	**Phase/°**
1	1	0	0	0	0
	2	0	0	0	0
	3	5.3677	13.5251	5.6267	−76.4749
	4	3.8535	13.5251	2.5276	−76.4749
2	1	0	0	0	0
	2	3.5366	13.5251	3.6588	−76.4749
	3	5.6847	13.5251	4.4955	−76.4749

In Table 2, a zero value indicates that the corresponding current source does not contribute to the current on the power line. It can be observed that the zero value occurs at bus 1; labels 1 and 2; and bus 2, label 1. This does not violate common sense as these are all labeled as loads that are

consuming active and reactive power and do not contribute to the power line current. Moreover, all of the traced active currents have the same phase angle regardless of how the current is traced from bus 1 or bus 2 in either direction. The same rationale applies to the reactive currents. This is also consistent with the fact that the voltages applied on the buses do not change when the current is decomposed into its traced components. The reactive current is 90 degrees out of phase from the active current, which complies with Equations (15) and (16).

It is observed that, if all of the traced currents from the same bus are summed, the result is equivalent to the total power line current. This proves the equivalence of the current tracing theory as the current tracing will not lose or generate new currents in addition to the line current.

4.2. SVM Results

In distribution systems with DERs, the fault current can be very small, as inverter-based DERs can only produce exceptionally small fault current contributions due to inverter current limiting action. Moreover, injected currents on different loads are continuously fluctuating in the normal condition. To obtain representative currents in the single line system, sample noises are injected to the specified load powers in Table 1 and the power flow is recalculated to obtain the traced current. This process is then repeated to obtain the load profile and a continuous currents curve. The injected noise follows the normal distribution such that,

$$X \sim N(\mu, \sigma^2), \tag{25}$$

where X represents active or reactive power sample noises; μ represents the average of the sample noises, which is set to 0; and σ stands for the standard deviation, which is set to 0.1. All the sample noises are independent from each other. The sample noises were injected cumulatively to the loads such that the kth point on the load profile is

$$P_k = P + \sum_{i=1}^{k} Xp_i, \tag{26}$$

$$Q_k = Q + \sum_{i=1}^{k} Xq_i, \tag{27}$$

where P_k and Q_k represent the active and reactive power of the kth point of the load profile, respectively; P and Q represent the given active and reactive power (Table 1); and Xp_i and Xq_i stand for the ith active or reactive power sample noises, respectively.

This process is repeated 500 times, and all of the parameters that are used for current tracing and SVM training purpose are recorded. In addition to sample noises, a small fault is also injected by increasing the active power consumption of bus 1, with current source 3 increased by 10% and decreasing the reactive power by 10% of the same current source. Again, the process is repeated 500 times, and all parameters are recorded. Only the traced current on the power line from bus 2 side is used as the current tracing kernel; however, it is the same as if the traced current from bus 1 side was used as the current tracing kernel, as in the conference paper [20]. The first 500 parameters are taken as normal condition, i.e., $y_i = -1$, and the last 500 parameters are considered as fault condition, i.e., $y_i = 1$. The penalty of misclassification C is set to be 1. Seventy percent of the parameters are randomly selected as the training data, and the remaining 30% are taken as the testing data. In this work, the non-waveform phasor current information is used for the fault identification problem. Other alternative measurement data have been considered in other research, such as exploiting sub-cycle waveform distortion features in pattern recognition algorithms as a part of the identification process [12,15].

The confusion matrix is used to represent the testing results as defined in [23]. The f-score, recall, and precision parameters are used to evaluate the performance of fault current identification based on the confusion matrix such that,

$$prec = \frac{tp}{tp + fp}, \tag{28}$$

$$rec = \frac{tp}{tp + fn}, \tag{29}$$

$$fs = 2\frac{prec * rec}{prec + rec}, \tag{30}$$

where *tp*, *fp*, *tn*, and *fn* represent true positive, false positive, true negative, and false negative, respectively.

To show the advantage of using the current tracing kernel, the fault current identification results using different feature spaces is compared. First, only the power line current $\vec{I}_L$ is used as the feature space. Then, the polynomial kernel, radial kernel, and current tracing kernel are added as the expanded feature space. All of the confusion matrices are calculated based on the same training and testing data. The confusion matrices and the performance based on the confusion matrices are shown in Tables 3 and 4, respectively.

Table 3. Confusion matrix using different feature space.

Feature Space		Fault	Normal
No Kernel	Predict Fault	tp = 90	fp = 61
	Predict Normal	fn = 13	tn = 136
Polynomial Kernel	Predict Fault	tp = 100	fp = 51
	Predict Normal	fn = 19	tn = 130
Radial Kernel	Predict Fault	tp = 95	fp = 56
	Predict Normal	fn = 16	tn = 133
Current Tracing Kernel	Predict Fault	tp = 145	fp = 6
	Predict Normal	fn = 0	tn = 149

Table 4. Performance using different feature space.

Feature Space	Precision	Recall	f1-Score
No Kernel	0.596	0.874	0.709
Polynomial Kernel	0.662	0.840	0.74
Radial Kernel	0.629	0.856	0.725
Current Tracing Kernel	0.96	1	0.98

It is clearly seen that among all the feature spaces used, the current tracing kernel has the best performance. All three performance parameters are significantly higher than the other feature spaces that were used. The recall value equals 1, which indicates that when there is a fault current on the power line; the SVM method using current tracing kernel will definitely detect it. In addition, the polynomial kernel and radial kernel have a better performance than if only $\vec{I}_L$ is used as feature space. However, the performance parameters do not increase significantly. When comparing with the results shown in [22], which have 97% overall accuracy, the overall current tracing kernel result in this paper has improved, i.e., an f1-score value of 98%.

5. Discussion

In the companion paper, it has been verified that the proposed tracing method is mathematically and physically identical to the original network. In this paper, the developed technique has been applied to a simple single power line system; however, it could be generalized to be as a part of a larger

distribution grid. Using the proposed CTM, pipelines of each current sources' contribution towards the fault currents were established in the form of virtually decomposed traced currents. The expanded features of the traced currents have the distinct advantage of containing more detailed information of the fault current, such as the change in contribution of each current source and the phase shift caused by the fault. These features can be exploited by the SVM algorithm for improved classification of faults, particularly where the fault levels are very low from the current limiting action of inverter-based DERs.

By choosing a large sample set of 1000 data points for faulted and normal cases, the proposed SVM method combined with the current tracing kernel is shown to be much more sensitive to very low-level faults on the power line compared to the polynomial and radial kernel methods, where the accuracy of detection was at most 74%. Compared to the other methods, such as the one in [22] where the accuracy of detection was at most 97%, the proposed method has improved accuracy of 98% while using significantly less measurement features.

These results are relevant in the context of smart grids aiming to improve distribution system state estimation, extending supervisory control and data acquisition processes beyond the substation domain as DERs proliferate. In these simulations, only the batch data is used for training and testing. However, the proposed model can be easily applied to practical streaming data obtained from intelligent electronic devices used in advanced metering infrastructure such as protection relays and phasor measurement units. With the enhanced features extracted through the proposed CTM, more intelligent protection relay coordination and fault isolation may be possible, particularly when considering multiple inverter-based DER operation from energy storage and renewable energy.

6. Concluding Remarks

In this paper, we propose a CTM augmented with SVM method to model and test a distribution feeder for power line fault current identification. The CTM modeled the distribution network by providing a detailed map of how current flows from each current source that is connected to one bus towards another source tied to a different bus. The proposed method does not violate any physical circuit laws. After applying the proposed current tracing, the virtual traced currents and the corresponding circuit are exactly equivalent to the original current and circuit. The traced current provides sufficient details and sensitivity for identifying faults and abnormal conditions in the distribution feeder. With these details, the feature space of the power line current is enlarged through the "current tracing kernel". In addition, the results proved and demonstrated the proposed method on a single power line distribution system, and the SVM method's performance was evaluated and compared by using different kernel methods. The results indicate that with the benefits of the proposed current tracing kernel, the SVM method is enhanced with more sensitivity to very low level faults compared to the commonly used kernel such as polynomial kernel and radial kernel.

The proposed method is a good fit for the distribution grid primary side overcurrent protection scheme. In the companion paper, the multicurrent sources to multicurrent source current tracing are already introduced, and they can be used to further expand the feature spaces of fault current. In the future, the authors will explore the implementation aspects of the proposed CTM described herein with the distribution grid backup protection scheme, especially the multicurrent sources to multicurrent sources case, which would undoubtedly occur with higher DER penetration in the future. Furthermore, in future work, the authors will explore how to implement and test this approach on a laboratory scale distribution test feeder to further verify the implementation of the SVM detection scheme using the proposed tracing method.

Author Contributions: Conceptualization, W.F.; methodology, W.F. and P.M.; software, W.F.; validation, W.F. and P.M.; formal analysis, W.F.; investigation, W.F.; resources, W.F.; data curation, W.F.; writing–original draft preparation, W.F.; writing–review and editing, P.M.; visualization, W.F.; supervision, P.M.; project administration, P.M.; funding acquisition, P.M.

Conflicts of Interest: The authors declare no conflicts of interest.

Abbreviations

The following abbreviations are used in this manuscript.

AI	Artificial Intelligence
CTM	Current Tracing Method
DER	Distributed Energy Resource
KNN	K-nearest Neighbors
SVM	Support Vector Machine

References

1. Saad, H.; Peralta, J.; Dennetiere, S.; Mahseredjian, J.; Jatskevich, J.; Martinez, J.; Davoudi, A.; Saeedifard, M.; Sood, V.; Wang, X.; et al. Dynamic averaged and simplified models for MMC-based HVDC transmission systems. *IEEE Trans. Power Deliv.* **2013**, *28*, 1723–1730. [CrossRef]

2. Daryabak, M.; Filizadeh, S.; Jatskevich, J.; Davoudi, A.; Saeedifard, M.; Sood, V.; Martinez, J.; Aliprantis, D.; Cano, J.; Mehrizi-Sani, A. Modeling of LCC-HVDC systems using dynamic phasors. *IEEE Trans. Power Deliv.* **2014**, *29*, 1989–1998. [CrossRef]

3. Runolfsson, T. On the dynamics of three phase electrical energy systems. In Proceedings of the IEEE American Control Conference (ACC), Boston, MA, USA, 6–8 July 2016; pp. 6827–6832.

4. Aravinthan, V.; Balachandran, T.; Ben-Idris, M.; Fei, W.; Heidari-Kapourchali, M.; Hettiarachchige-Don, A.; Jiang, J.N.; Lei, H.; Liu, C.C.; Mitra, J.; et al. Reliability modeling considerations for emerging cyber-physical power systems. In Proceedings of the 2018 IEEE International Conference on Probabilistic Methods Applied to Power Systems (PMAPS), Boise, ID, USA, 24–28 June 2018; pp. 324–330.

5. Davis, K.R.; Davis, C.M.; Zonouz, S.A.; Bobba, R.B.; Berthier, R.; Garcia, L.; Sauer, P.W. A cyber-physical modeling and assessment framework for power grid infrastructures. *IEEE Trans. Smart Grid* **2015**, *6*, 2464–2475. [CrossRef]

6. Fei, W.; Jiang, J.N.; Wu, D. Impacts of Modeling Errors and Randomness on Topology Identification of Electric Distribution Network. In Proceedings of the 2018 IEEE International Conference on Probabilistic Methods Applied to Power Systems (PMAPS), Boise, ID, USA, 24–28 June 2018; pp. 1–6.

7. Ji, G.; Sharma, D.; Fei, W.; Wu, D.; Jiang, J.N. A Graph-theoretic Method for Identification of Electric Power Distribution System Topology. In Proceedings of the 1st Global Power, Energy and Communication Conference (GPECOM), Nevsehir, Turkey, 12–15 June 2019; pp. 403–407.

8. Garces, A. A linear three-phase load flow for power distribution systems. *IEEE Trans. Power Syst.* **2016**, *31*, 827–828. [CrossRef]

9. Yang, J.; Zhang, N.; Kang, C.; Xia, Q. A state-independent linear power flow model with accurate estimation of voltage magnitude. *IEEE Trans. Power Syst.* **2017**, *32*, 3607–3617. [CrossRef]

10. Vita, V.; Ekonomou, L.; Christodoulou, C.A. The impact of distributed generation to the lightning protection of modern distribution lines. *Energy Syst.* **2016**, *7*, 357–364. [CrossRef]

11. Fei, W.; Ji, G.; Sharma, D.; Jiang, J.N. A New Traveling Wave Representation for Propagation of Energy Transients in Power Lines from a Quantum Perspective. In Proceedings of the North American Power Symposium (NAPS), Fargo, ND, USA, 9–11 September 2018; pp. 1–6.

12. Pavlatos, C.; Vita, V. Linguistic representation of power system signals. In *Electricity Distribution*; Springer: Berlin, Germany, 2016; pp. 285–295.

13. Harrou, F.; Taghezouit, B.; Sun, Y. Improved *k* NN-Based Monitoring Schemes for Detecting Faults in PV Systems. *IEEE J. Photovolt.* **2019**, *9*, 811–821. [CrossRef]

14. Abid, F.B.; Zgarni, S.; Braham, A. Distinct bearing faults detection in induction motor by a hybrid optimized SWPT and aiNet-DAG SVM. *IEEE Trans. Energy Convers.* **2018**, *33*, 1692–1699. [CrossRef]

15. Pavlatos, C.; Vita, V.; Dimopoulos, A.C.; Ekonomou, L. Transmission lines' fault detection using syntactic pattern recognition. *Energy Syst.* **2019**, *10*, 299–320. [CrossRef]

16. Guo, M.F.; Zeng, X.D.; Chen, D.Y.; Yang, N.C. Deep-learning-based earth fault detection using continuous wavelet transform and convolutional neural network in resonant grounding distribution systems. *IEEE Sens. J.* **2017**, *18*, 1291–1300. [CrossRef]

17. Park, J.D.; Candelaria, J.; Ma, L.; Dunn, K. DC ring-bus microgrid fault protection and identification of fault location. *IEEE Trans. Power Deliv.* **2013**, *28*, 2574–2584. [CrossRef]

18. Vaseghi, B.; Takorabet, N.; Meibody-Tabar, F. Fault analysis and parameter identification of permanent-magnet motors by the finite-element method. *IEEE Trans. Magn.* **2009**, *45*, 3290–3295. [CrossRef]

19. Cheng, F.; Peng, Y.; Qu, L.; Qiao, W. Current-based fault detection and identification for wind turbine drivetrain gearboxes. *IEEE Trans. Ind. Appl.* **2016**, *53*, 878–887. [CrossRef]

20. Fei, W.; Moses, P. Modeling Power Distribution Grids through Current Tracing Method. In Proceedings of the IEEE International Conference on Smart Energy Grid Engineering (SEGE), Oshawa, ON, Canada, 12–14 August 2019; pp. 196–200.

21. James, G.; Witten, D.; Hastie, T.; Tibshirani, R. *An Introduction to Statistical Learning*; Springer: Berlin, Germany, 2013; Volume 112.

22. Zhang, Y.; Ilic, M.D.; Tonguz, O.K. Mitigating blackouts via smart relays: A machine learning approach. *Proc. IEEE* **2010**, *99*, 94–118. [CrossRef]

23. Sammut, C.; Webb, G.I. *Encyclopedia of Machine Learning and Data Mining*; Springer Publishing Company, Incorporated: Berlin, Germany, 2017.